Close look at charge carrier injection in polymer field-effect transistors

L. Bürgi, T. J. Richards, R. H. Friend, and H. Sirringhaus

Citation: Journal of Applied Physics **94**, 6129 (2003); doi: 10.1063/1.1613369
View online: http://dx.doi.org/10.1063/1.1613369
View Table of Contents: http://scitation.aip.org/content/aip/journal/jap/94/9?ver=pdfcov
Published by the AIP Publishing

Close look at charge carrier injection in polymer field-effect transistors

L. Bürgi, T. J. Richards, R. H. Friend, and H. Sirringhaus[a)]
Cavendish Laboratory, Madingley Road, Cambridge CB3 0HE, United Kingdom

(Received 26 June 2003; accepted 5 August 2003)

Parasitic contact resistance effects are becoming a major issue in organic transistors in that they can severely limit or even dominate their overall transistor performance. We present a systematic study of the contact resistance in bottom-contact polymer field-effect transistors made from poly(3-hexylthiophene) (P3HT) as well as poly-9,9′dioctyl-fluorene-co-bithiophene (F8T2). A microscopic approach based on noncontact scanning-probe potentiometry was used to directly separate the transport properties of the transistor channel and the electrode/polymer contacts, giving very accurate experimental access to both the source and drain contact resistance. The influence of the relevant parameters (temperature, electrode work function, ionization potential of the polymer, charge carrier mobility) on the source/drain contact resistance is investigated. We find that for ''good'' source/drain contacts that give rise to relatively small overall contact resistances ($\leqslant$50 kΩ cm), e.g., P3HT with chromium–gold electrodes, the source and the drain contact resistances are almost identical and are governed by bulk transport through the conjugated polymer. However, for ''bad'' contacts with a Schottky barrier for hole injection $\varphi_b \geqslant 0.3$ eV, e.g., F8T2 with gold electrodes, the source contact resistance is considerably larger than the drain contact resistance and is dominated by charge-carrier injection at the source. Surprisingly small activation energies of 60–140 meV have been found for the source contact resistance, which are smaller than both φ_b and the activation energy of the mobility. From this we conclude that the commonly assumed (diffusion-limited) thermionic-emission models do not adequately describe the charge injection process in bottom-contact polymer transistors. On the basis of our results we propose a simple model, in which the source contact resistance is assumed to be the sum of resistance arising from the injection process and resistance due to bulk transport through a depletion region, whereas only the latter contributes to the drain contact resistance. © *2003 American Institute of Physics.*
[DOI: 10.1063/1.1613369]

I. INTRODUCTION

The performance of thin-film field-effect transistors (TFTs) based on conjugated organic materials as the active semiconducting component has experienced impressive improvement in recent years.[1] So far, much of the scientific effort has been directed towards larger field-effect mobilities. Better organic materials and refined transistor processing technologies have resulted in mobilities of a few $cm^2/V\,s$ for vacuum-deposited conjugated oligomers such as pentacene, whereas the best values for solution-processed conjugated polymers are in the range of 10^{-1} $cm^2/V\,s$.[1] New device architectures, some of them fully exploiting the unique material properties of organic materials, have also been explored, with emphasis on transistor designs with shorter channel lengths.[2,3] All these activities are to a large extent motivated by the need to achieve transistor switching speeds and drive currents that comply with low-end applications such as, e.g., active matrix displays.

Despite this considerable progress, comparatively little effort has been made to investigate contact effects in organic transistors. Consequently, the charge injection/extraction process at the source/drain electrodes is still relatively poorly understood. This is somewhat surprising since contact resistances in organic transistors are with typically 10 kΩ cm–10 MΩ cm[4–17] large compared to their inorganic counterparts, which is due to the fact that the source and drain contacts in organic TFTs are not easily optimized by conventional processes such as selective semiconductor doping. Contact effects are thus expected to seriously affect organic transistors, especially in drive-current optimized short-channel devices. This is underscored by several reports of (completely) contact-limited organic transistors,[3,9,12,15,16] in which transistor action, i.e., the modulation of the source–drain current by the gate voltage, is not due to modulation of the channel resistance but due to variation of the contact resistance with the gate voltage. A simple criterion for contact limitation in a transistor of field-effect mobility μ and contact resistance R_c can be obtained from the following consideration: The contact resistance is to good approximation independent of the channel length L, but the actual channel resistance scales with L and in the linear regime is given by $R_{ch}=L/W\mu en$ (where n is the areal density of accumulated charge). Therefore, a critical channel length $L_c=\mu en R_c$ can be defined for which $WR_{ch}=R_c$ so that the contacts and the channel contribute equally to the total transistor resistance. Only transistors with a channel length clearly larger than L_c can be expected to show ''clean'' TFT operation. Transistors with channel lengths such that $L \leqslant L_c$ become (severely) contact

a)Author to whom correspondence should be addressed; electronic mail: hs220@phy.cam.ac.uk

limited, meaning that the source–drain voltage mainly drops over the contact regions rather than over the transistor channel and the overall transistor current is reduced accordingly. Inserting typical values for polythiophene[13] ($\mu = 10^{-2}$ cm^2/V s, $R_c = 50$ kΩ cm, $n = 2\times10^{12}$ cm^{-2}) yields $L_c \approx 2$ μm. This example illustrates that one has to carefully deal with the contact resistance in organic transistors even for moderate channel lengths and even in the case of materials with relatively low ionization potentials (5 eV for polythiophene) where barriers to injection of holes are low and, consequently, contact resistances comparatively small. We note here that most polymers that are potentially attractive for transistor applications, e.g., polyfluorene-based materials, exhibit ionization potentials larger than 5.3 eV, which makes them less prone to doping by ambient oxygen, but results in strong contact effects. As an example, for poly-9,9′dioctyl-fluorene-co-bithiophene (F8T2) with contact resistances larger than MΩ cm,[11] estimated critical channel lengths are $L_c > 10$ μm.

It is clear from the above that efforts to develop new device architectures aimed at improved switching speeds and drive currents of organic transistors in general, and new short-channel (<1 μm) transistor structures in particular,[2,3] must be backed by efforts to understand the physics behind the contact resistance and possibly reduce or even eliminate the problems associated with it. The field has progressed to a point where charge injection, long known to play a crucial role in organic light-emitting diodes,[18] is becoming a major issue for organic transistors too.

Contact effects in organic transistors have been studied experimentally in TFTs based on vacuum-deposited oligomers (oligothiophenes,[5,6,8,9,12] pentacene[10,15–17]), solution-processed polymers (polythiophene,[7,13] F8T2[3,11,14]) as well as by two-dimensional (2D) device modeling.[19–21] In the majority of the experimental studies the total contact resistance was estimated by analyzing the (macroscopic) electrical device characteristics using more or less stringent assumptions such as ohmic resistance,[5–7,15,17] electric-field independence of R_c,[3,11] complete contact limitation,[9] or using simplified transistor models with many fit parameters.[10,14,16] Only Chwang and Frisbie[9] have so far addressed the effect of temperature, which of course is a key parameter in connection with charge injection. Those studies going beyond a sole estimation/quantification of the contact effects all assumed[10,14,16,19–21] or concluded[9] that (diffusion-limited) thermionic emission is the dominant process for injection of charge carriers in organic transistors. In anticipation of the discussion in Sec. IV we would like to point out that the results presented here clearly challenge this assumption in the case of bottom-contact polymer TFTs.

Recently, scanning-probe potentiometries have been successfully applied to organic materials.[12,13] They give very direct insight into the mesoscopic functioning of optoelectronic devices in that they reveal the electrostatic potential landscape inside operating devices with very high (<100 nm) spatial resolution. In terms of charge injection knowledge of the internal electrostatic potential is obviously a big asset since it allows an elegant experimental disentanglement of bulk and contact effects. This is especially true for metal/organic semiconductor contacts for which electrical characteristics are not easily accessible from macroscopic measurements since they are often obscured by transport through the low-mobility bulk.

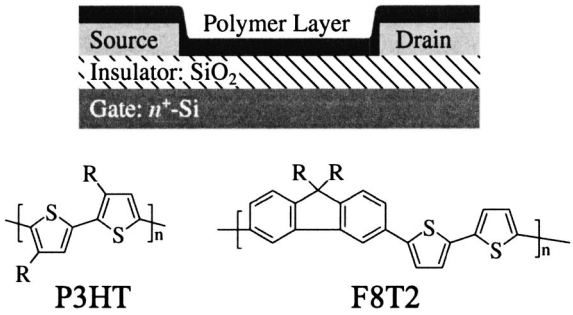

FIG. 1. Schematic diagram of the bottom-contact field-effect transistors. The chemical structures of the polymers are also shown. The rest group R refers to a hexyl (C_6H_{13}) and an octyl (C_8H_{17}) group for P3HT and F8T2, respectively.

In this article we use such a microscopic approach, noncontact potentiometry,[13] for a very direct and complete characterization of the electrical properties of both the source and the drain contacts in bottom-contact polymer TFTs based either on poly(3-hexylthiophene) (P3HT) or F8T2 (Fig. 1). P3HT and F8T2 have been chosen not only because they are today the most widely used conjugated polymers for transistor applications, but also because their ionization potentials of 5.0 and 5.5 eV, respectively, are substantially different. We have systematically investigated the dependence of the source/drain contact $I-V$ characteristics on the temperature, Schottky barrier for hole injection (φ_b), and charge carrier density. The contact interface energetics (Schottky barrier) was controlled via the ionization potential of the polymer and by using different metals as source/drain electrodes (Au, Ag, Cu, Cr, Al). Importantly, by varying the temperature the charge carrier mobility could be tuned over up to five decades without having to resort to a variety of different materials and thereby the influence of carrier mobility on the contact resistance[22] could be addressed most directly.

II. EXPERIMENTAL METHODS

The experiments were performed on standard bottom-contact transistors with photolithographically patterned source/drain metal electrodes (Fig. 1), i.e., a device structure that is widely used in, and thus relevant to, organic semiconductor research and technology. The transistors were fabricated on n^+-Si wafers (gate electrode) with a 210 nm thick high-quality thermal SiO_2 oxide layer ($C_i = 16$ nF/cm^2). After careful cleaning of the substrates (ultrapure water, acetone, isopropanol, exposure to O_2 plasma) 30–35 nm thick films of Au, Ag, Cu, Cr, Al (all better than 99.99% purity), or 180 nm Au with a 15 nm Cr adhesion layer (Cr–Au) were deposited by thermal evaporation at a rate of ≈0.3 Å/s in high vacuum (10^{-6} mbar). Photolithography combined with wet etching was then used to define interdigitated source/drain electrodes of various channel lengths (up to 20 μm) and $W = 1$ cm channel width. Subsequently, the substrates were again carefully cleaned, including exposure to O_2

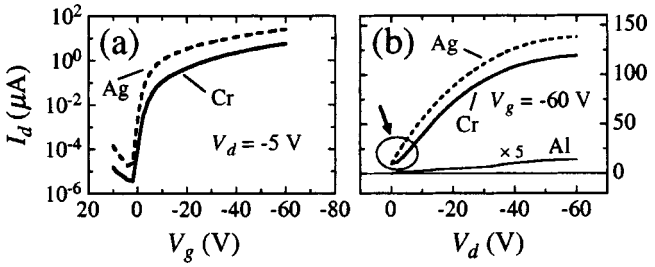

FIG. 2. (a) Transfer and (b) output characteristics of typical P3HT thin-film transistors with Ag (dashed line), Cr (solid line), or Al (thin solid line) electrodes ($L=22\ \mu\text{m}, W=1\ \text{cm}, T=300\ \text{K}$). High work function electrodes, e.g., Ag, result in good *p*-type transistors with field-effect mobilities of $\approx 10^{-2}\ \text{cm}^2/\text{V s}$, on/off current ratios of better than 10^5, and subthreshold slopes of ≈1 V/decade. Note that the scale for the output characteristics of Al is expanded (5×). For clarity Ag and Cr output characteristics are offset by 10 μA in (b).

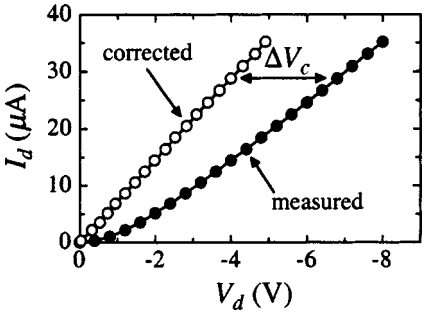

FIG. 3. Measured output characteristic of a P3HT transistor with Cu source/drain electrodes ($L=4.5\ \mu\text{m}, W=0.9\ \text{cm}, V_g=-30\ \text{V}, T=300\ \text{K}$). The open symbols show the output characteristic after correction for contact effects, i.e., the $I-V$ curve of the channel alone.

plasma (Au, Cr–Au), dipping in buffered hydrofluoric acid (Au, Ag, Cr–Au, Cu, and Cr) and/or nitric acid (Au, Cr–Au, Cr, and Al), in this sequence.

For P3HT transistors the clean silicon oxide was then derivatized with hexamethyldisilazane (HMDS) by exposing the substrates to saturated HMDS vapor at ≈160 °C for several hours.[23] Subsequently, 25–40 nm thick films of the active material, regioregular (>98%) head to tail coupled poly(3-hexylthiophene) synthesized according to the method of McCullough and co-workers,[24] were then deposited by spin coating from a ≈0.3 wt % solution in anhydrous chloroform. Finally, the P3HT devices were annealed at 100 °C in vacuum (10^{-6} mbar) for 10 h. These processing conditions result in stable P3HT transistors with a mobility of $\approx 10^{-2}\ \text{cm}^2/\text{V s}$, turn-on voltages between +3 and 0 V, and on/off current ratios exceeding 10^5 (Fig. 2).

In the case of F8T2 transistors a self-assembled monolayer of 1*H*,1*H*,2*H*,2*H*-perfluorodecyltrichlorosilane (FDTS) was deposited on the silicon oxide by placing the substrates in an evacuated desiccator and exposing them to saturated vapor of FDTS at room temperature for 12 h. To complete the devices, 60 nm thick films of F8T2 were then spin coated from a 0.8 wt % solution in anhydrous xylene (mixed isomers). For F8T2 we found that using FDTS instead of HMDS as the silylating agent dramatically reduced bias-stress effects in bottom-contact transistors, which is in agreement with work by Salleo *et al.*[25] who observed similar improvement using a slightly different fluorinated silane. Overall, our F8T2 transistors show a mobility of 10^{-3}–$5\times 10^{-3}\ \text{cm}^2/\text{V s}$, turn-on voltages between +4 and −5 V, and on/off current ratios better than 10^6. To minimize unintentional doping all processing and measurement steps that involved P3HT and F8T2 were carried out in inert N_2 atmosphere or vacuum.

The local electrostatic potential in the channel of operating transistors was measured using noncontact potentiometry, a nondestructive scanning-probe technique with ≈100 nm resolution. Noncontact potentiometry was performed using a noncontact scanning-force microscope in scanning Kelvin probe mode based on the frequency modulation technique in ultrahigh vacuum (UHV). In this mode the voltage applied to the conducting tip[26] is driven by a feedback loop and takes on the value of the local surface potential which essentially follows the electrostatic potential in the accumulation layer of the TFT. Details of our experimental setup are published elsewhere.[13] The potential profiles shown in this article have been corrected for differences in the work function of the tip and sample by subtracting a "background" profile obtained with no voltage applied between the source and drain.[13]

Current–voltage characteristics of the transistors were acquired with a Hewlett Packard 4145B semiconductor parameter analyzer. During noncontact potentiometry measurements in the UHV system the transistors were driven and the transistor currents monitored using an Agilent 6614C power supply and a Keithley 6517A electrometer. The sample temperature was measured with a calibrated Si diode. Throughout this study gate and drain voltages are given with respect to the grounded source.

III. RESULTS

Typical macroscopic fingerprints of contact limited P3HT transistors are displayed in Fig. 2. Whereas using Ag source/drain electrodes results in perfect transistor operation, Cr shows moderate contact limitation with strong current suppression at low drain voltages clearly seen when, e.g., comparing the transfer characteristics of Ag and Cr in Fig. 2(a), and Al is severely contact limited with virtually no current flowing through the highly resistive electrode/polymer contacts. The key feature of contact resistance is the nonlinear increase of the output characteristics at low drain voltages, highlighted by an arrow in Fig. 2(b) and also clearly seen in Fig. 3, which shows an expanded output characteristic of a P3HT transistor with Cu electrodes. Note that the presence of such nonohmic contact resistance reduces transistor currents considerably in the low drain-bias regime.

Microscopically the contact resistance manifests itself in abrupt voltage drops ΔV_s and ΔV_d in the source and drain contact regions, respectively. This can be clearly seen in Fig. 4, which shows typical potential profiles for a representative selection of TFTs studied here. Cr–Au electrodes form a relatively good contact for P3HT as evidenced by the rather small contact voltage losses in Fig. 4(a). Interestingly, however, ΔV_s and ΔV_d, and therefore the source and drain contact resistance, are nearly equal in the case of

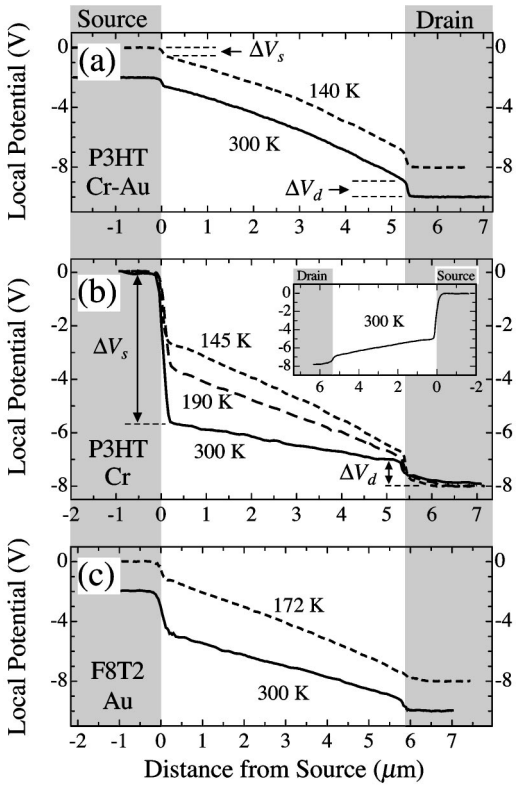

FIG. 4. Profiles of the electrostatic potential across the channel of operating transistors. (a) P3HT transistor with Cr–Au source/drain electrodes ($L \approx 5.3\ \mu\text{m}, V_g = -20\ \text{V}, V_d = -8\ \text{V}$). The profile taken at 300 K is offset by -2 V for clarity. (b) Profiles of an $L \approx 5.5\ \mu$m P3HT transistor with Cr electrodes taken at three different temperatures ($V_g = -40\ \text{V}, V_d = -8\ \text{V}$). The inset of (b) shows a profile obtained after switching the source and drain on the same TFT ($V_g = -40\ \text{V}, V_d = -8\ \text{V}$). (c) F8T2 transistor with Au source/drain electrodes ($V_g = -40\ \text{V}, V_d = -8\ \text{V}$). The profile taken at 300 K is offset by -2 V.

P3HT/Cr–Au.[13] At first glance this is somewhat counterintuitive since in the simple flat-band picture normally assumed for undoped conjugated polymers one would expect a barrier for injection of charge carriers at the source but no barrier for extraction, and therefore no contact voltage drop at the drain. This point will be addressed in Sec. IV.

For transistors with a relatively large Schottky barrier for injection, φ_b, the situation is different as can be seen in Figs. 4(b) and 4(c), which show potential profiles taken of a P3HT transistor with Cr electrodes and an F8T2 transistor with Au electrodes, respectively (in both cases $\varphi_b \approx 0.3$ eV). Since φ_b is used here only for qualitative discussion rather than for quantitative analysis its value in the *p*-type material is assumed to be $\varphi_b = I - W_m$ where the ionization potential I is 5.0 eV for regioregular P3HT and 5.5 eV for F8T2, and W_m is the measured work function of the source/drain electrodes (Table I).[27] The profiles in Figs. 4(b) and 4(c) are representative of the class of profiles taken of transistors with $\varphi_b \geqslant 0.3$ eV (see Table I). They show pronounced asymmetry between the source and drain: A considerably larger voltage is needed to inject the holes at the source than to extract them at the drain ($\Delta V_s > \Delta V_d$). We point out that this asymmetry is not due to one of the two electrodes forming better contact with the polymer than the other, since upon switching source and drain electrodes we obtain nearly identical results as can be verified by comparing the 300 K profile in Fig. 4(b) with the profile in the inset. Measured asymmetries are summarized in Fig. 5(a). The source/drain asymmetry decreases with an increase in the density of induced charge carriers (i.e., with increasing $|V_g|$) and with decreasing Schottky barrier φ_b. A surprising feature of the profiles in Figs. 4(b) and 4(c) is that as the temperature is lowered, less and less voltage drops over the contacts and consequently a

TABLE I. Source contact resistance R_s of bottom-contact P3HT and F8T2 transistors made with different metal electrodes ($T = 300$ K, $V_g = -20$ V). The measured work functions W_m and estimated Schottky barrier heights φ_b are also given. W_m was measured with the scanning Kelvin probe microscope on the electrodes of fully treated transistor substrates just prior to the deposition of the polymer layer. All work functions were measured with respect to a Au reference electrode, for which a value of 5.2 eV (from standard literature) is assumed. For pure Au electrodes no measurable $\Delta V_{d,s}$ was observed, leaving us with an upper limit for the contact resistance in this case. The gray shading denotes transistors with asymmetry between the source and drain contact resistance, i.e., $R_s > R_d$. (No potential profiles were acquired for P3HT/Al transistors and therefore no statement can be made as to the asymmetry.)

Polymer	Electrode	W_m (eV)	φ_b (eV)	R_s (kΩ cm)
P3HT	Au	5.2	0.0	<5
P3HT	Ag	4.89±0.10	0.1	≈15
P3HT	Cr–Au			22
P3HT	Cu	4.72±0.10	0.3	320
P3HT	Cr	4.68±0.10	0.3	5400
F8T2	Au	5.2	0.3	13 000
F8T2	Cr–Au			>70 000
P3HT	Al	4.05±0.10	1.0	∞

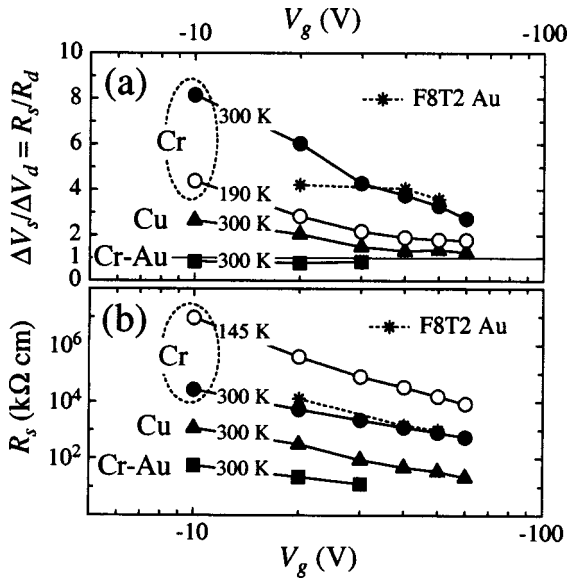

FIG. 5. (a) Source/drain asymmetry as a function of the gate voltage at 300 K (closed symbols) and at reduced temperature (open symbols). Circles, triangles, and squares represent P3HT transistors with Cr, Cu, and Cr–Au electrodes, respectively. Room temperature data for F8T2 with Au electrodes are also shown (stars). (b) Gate–voltage dependence of the source contact resistance. Assuming a power law dependence, $R_s \propto |V_g|^{-m}$ yields, e.g., $m = 1.3$, 1.6, and 2.1 and $m = 2.3$, 3.2, and 4.5, at $T = 300$, 190, and 145 K for P3HT transistors with Cr–Au and Cr electrodes, respectively.

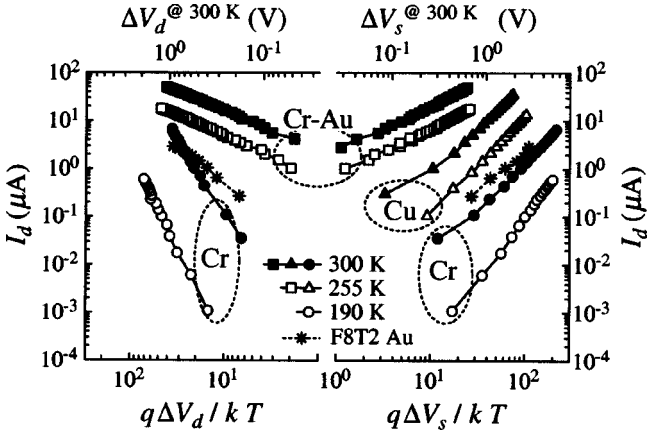

FIG. 6. Contact current–voltage characteristics at 300 K (closed symbols) and at reduced temperature (open symbols). Circles, triangles, and squares represent P3HT transistors with Cr, Cu, and Cr–Au electrodes, respectively ($V_g=-30$ V). The stars depict room temperature data for F8T2 with Au electrodes ($V_g=-40$ V). For clarity some drain characteristics are not displayed. Note that I_d is plotted as a function of the reduced voltage $qV_{s/d}/kT$. For comparison the upper abscissa shows the measured voltages at 300 K. Fitting the source contact characteristics with $I_d \propto \Delta V_s^n$ yields, e.g., $n=1.0$, 2.0, and 2.2 for P3HT transistors with Cr–Au, Cu, and Cr electrodes at 300 K, respectively.

larger portion ΔV_{ch} of the drain voltage is available over the channel. One could therefore say that the transistors become more ideal (less contact limited) as the temperature is lowered. From this somewhat counterintuitive result we infer that for transistors with $\varphi_b \geqslant 0.3$ eV the temperature dependence of the contact resistance is weaker than that of the channel resistance $R_{\mathrm{ch}}(T)=L/W\mu(T)C_i|V_g|$, the latter being dominated by the field-effect mobility of the polymers, which show an activation energy of the order of 100–160 meV. We will come back to this intriguing property later.

A key advantage of using potentiometry in this context is the ability to access the current–voltage characteristics of the source/polymer and the polymer/drain *contacts* most directly: $\Delta V_{s/d}$ obtained from the microscopic potential profiles is plotted versus the simultaneously measured drain current with V_d being the implicit parameter that is varied during the experiment. Typical examples of such $I-V$ curves are given in Fig. 6. Clearly, the contact characteristics are generally nonohmic[9,14] and the commonly made assumption of linear contact $I-V$ characteristics[5–7,15] is not justified in polymer TFTs with $\varphi_b \geqslant 0.3$ eV. When plotted not versus $\Delta V_{s/d}$ itself but rather versus $q\Delta V_{s/d}/kT$ as in Fig. 6, the $\log I$–$\log V$ curves of a given electrode material at different temperatures appear to be just vertically offset, and the functional form of I_d could therefore be expressed as $I_d=g(T)\times f(q\Delta V_{s/d}/kT)$, as implied by Necliudov *et al.*[10,16] However, using the functional form assumed by Necliudov *et al.*, a "leaky Schottky diode" with $f(x)=\exp(x/\eta)$ where η is the ideality factor, to fit our contact $I-V$ curves results in values of $\eta>30$ which are unphysically large, and therefore this simple model does not account for the contacts of our polymer TFTs.

Knowing the source/drain contact $I-V$ characteristics allows one to correct measured transistor characteristics for contact effects. A typical example of such a corrected output characteristic is depicted by the open symbols in Fig. 3. To obtain the corrected characteristic the total contact voltage drop $\Delta V_c(I_d)=\Delta V_s(I_d)+\Delta V_d(I_d)$ (a positive number) is added to the overall drain voltage $V_d(I_d)$ (a negative number) to yield the actual potential $\Delta V_{\mathrm{ch}}=V_d+\Delta V_c$ available over the channel. I_d is then plotted as a function of ΔV_{ch}, resulting in the $I-V$ curve of the channel alone. As seen in Fig. 3, corrected output characteristics are strictly linear at low drain voltages. Furthermore, the linear field-effect mobility extracted from the corrected output characteristic of Fig. 3 is, with 7.5×10^{-3} cm^2/V s, in excellent agreement with the real field-effect mobility of 7.2×10^{-3} cm^2/V s determined from potential profiles $V(x)$ using $I_d=W\mu C_i[V_g-V(x)]\partial V/\partial x$.[13] Note that the field-effect mobility obtained by fitting a linear function to the measured, uncorrected output characteristic is, with 4.2×10^{-3} cm^2/V s, almost a factor of 2 smaller. This underlines the fact that one has to be extremely careful when trying to extract meaningful linear field-effect mobilities from transistor characteristics,[15,17] even in the case of only relatively mild contact effects, e.g., those present in the P3HT/Cu transistor in Fig. 3.

Figure 6 confirms that the contact $I-V$ curves, and thus the contact resistance, depend crucially on the electrode material used. The measured contact resistances, summarized in Table I, clearly depend on the electrode work function (compare the P3HT data for different electrodes) as well as on the ionization potential of the polymer (P3HT and F8T2 transistors with Au electrodes). Moreover, there is a clear correlation between the estimated Schottky barrier height φ_b and the contact resistance. (We use

$$R_{s,d}=W\left.\frac{\Delta V_{s,d}}{I_d}\right|_{V_d=-3\mathrm{V}}$$

to determine contact resistances. This definition is versatile enough to allow straightforward comparison between different materials.) The fact that P3HT transistors with Cu and Cr electrodes exhibit different contact resistance despite Cu and Cr having very similar measured work functions is tentatively ascribed to contributions from interfacial dipole layers altering the energy barrier φ_b by a small amount δ.[28] We would like to mention that our microscopic contact resistances are in good agreement with estimates derived from channel-length dependent studies,[29,30] which we performed on transistors with different, 2–20 μm channel lengths fabricated on a single Si substrate (data not shown). Also, our contact resistances compare favorably with values given in the literature: For P3HT bottom-contact transistors with Cr–Au electrodes Sirringhaus *et al.*[7] derived a total R_c of 10–40 kΩ cm, and for F8T2 with Au electrodes values for R_c of 5–10 MΩ cm have been estimated.[11,14] As is clear from Fig. 5(b), the contact resistance decreases with an increase in gate voltage $|V_g|$, i.e., with an increase in charge carrier density $n=C_i|V_g|/e$, which is in qualitative agreement with published results on organic[5,7,9,12,14,15,17] as well as on α-Si (Refs. 29 and 30) TFTs. The dependence of R_s on the charge carrier density is found to be stronger for TFTs with large overall contact resistance, that is, for transistors with large φ_b. As expected, the contact resistance is greatly

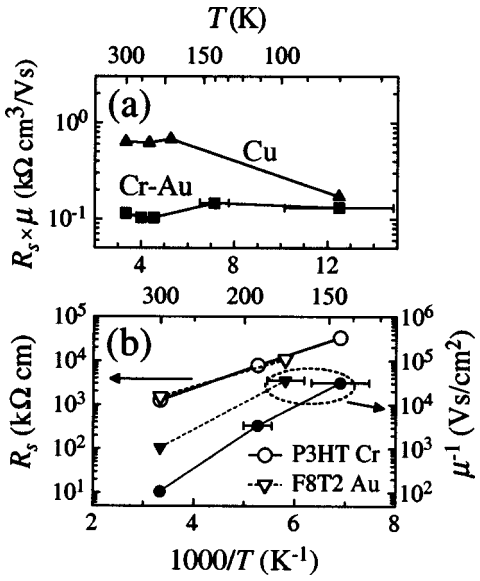

FIG. 7. Temperature dependence of the contact resistance. (a) Product of the source contact resistance and field-effect mobility as a function of the inverse temperature for P3HT transistors with Cr–Au and Cu electrodes ($V_g = -30$ V). (b) Source contact resistance (open symbols) and inverse field-effect mobility (closed symbols) as a function of the inverse temperature ($V_g = -40$ V). Circles and triangles represent P3HT/Cr and F8T2/Au transistors, respectively. As an example, for P3HT/Cr transistor activation energies of 81 ± 10 and 149 ± 17 meV are deduced for R_s and μ, respectively. (For simplicity only selected, representative error bars are plotted.)

affected by the temperature and increases rapidly with a decrease in temperature as is apparent in Fig. 5(b) as well as in Fig. 6.

The key result of this study is shown in Fig. 7, which summarizes the temperature dependence of the contact resistance in our bottom-contact polymer TFTs. Overall, we find that the dependence of R_s is consistent with an activated behavior above ≈ 140 K ($R_s \propto \exp[\Delta_R/kT]$) with surprisingly small, gate-voltage dependent activation energies Δ_R of 60–140 meV. These values are comparable to or even smaller than the corresponding activation energies $\Delta_\mu = 100$–160 meV, which we deduce for the field-effect mobility. ($\mu \propto \exp[-\Delta_\mu/kT]$ with a V_g-dependent Δ_μ. Δ_μ showed significant variation between identically prepared samples, an effect previously observed in organic TFTs.[31] This is likely due to a delicate dependence of the density of trapped states at the insulator/semiconductor interface on so far uncontrolled processing parameters. All field-effect mobilities have been determined directly from potential profiles $V(x)$ using $I_d = W\mu C_i[V_g - V(x)]\partial V/\partial x$.[13])

Importantly, for transistors with low contact resistance we find that the product of contact resistance and field-effect mobility, $R_s \times \mu$, is independent of the temperature as can be clearly seen in the case of P3HT with Cr–Au electrodes in Fig. 7(a). Considering the fact that the mobility as well as the contact resistance vary by almost five orders of magnitude over the available temperature range, we conclude that the contact resistance is dominated by the charge carrier mobility of the conjugated polymer and strictly follows $R_s \propto \mu^{-1}$ in this case. For transistors of intermediate contact resistance with $\varphi_b \approx 0.3$ eV there is a crossover [P3HT with Cu electrodes in Fig. 7(a)] to a regime for $\varphi_b \geqslant 0.3$ eV where the source contact resistance is significantly *less* temperature dependent than the mobility [Fig. 7(b)]. In this latter regime we find gate-voltage dependent activation energies of R_s that vary from $\Delta_R = 106 \pm 12$ meV at $V_g = -20$ V to $\Delta_R = 70 \pm 9$ meV at $V_g = -60$ V for P3HT with Cr electrodes. (For comparison, the corresponding activation energy of the mobility at $V_g = -60$ V is $\Delta_\mu = 139 \pm 16$ meV.) In the case of F8T2 with Au electrodes the activation energy at $V_g = -40$ V is $\Delta_R = 68 \pm 11$ meV ($\Delta_\mu = 122 \pm 19$ meV). As seen in Fig. 7(b), there is striking agreement between the results obtained for the two very different polymer TFTs P3HT/Cr and F8T2/Au with, however, similar Schottky barrier heights φ_b for the injection of holes. We emphasize that in the large-barrier regime ($\varphi_b \geqslant 0.3$ eV) the activation energies of the contact resistance are not only smaller than Δ_μ, but they are significantly smaller than the estimated Schottky barrier height φ_b.

IV. DISCUSSION

On the basis of our results we now examine the possible origin of the contact resistance effects observed in bottom-contact polymer TFTs.

First of all we address the effect of surface oxides, most likely present on all but the Au electrodes. One might expect that transport through the bulk of such oxides could (seriously) affect the contact resistance. However, we have direct experimental evidence that the transport process through surface oxides plays only a minor role as detailed in the following. Let us first consider TFTs with good contacts (e.g., P3HT/Cr–Au). In this case the contact resistance is dominated by the mobility of the *polymer* [Fig. 7(a)], i.e., a material property of the polymer, and no transport mechanism through the bulk of the oxide layer can be thought of that would explain this result. Then, for the other class of transistors with $\varphi_b \geqslant 0.3$ eV the large asymmetry between the source and drain [Fig. 5(a)] rules out bulk transport through the oxide since the latter would lead to symmetric contact resistances (at least at low drain voltages). Also, the results obtained for P3HT transistors with Cr electrodes, where one would expect a thin surface oxide on the reactive chromium, agree perfectly well with the results obtained for F8T2 transistors with pure Au electrodes, where no surface oxide is present. These reasons as well as the fact that the contact resistance and the asymmetry between the source and drain clearly correlate with the difference in electrode work function and ionization potential of the polymer, φ_b (Table I), lead us to the conclusion that bulk transport through insulating barriers due to surface oxides does not contribute significantly to the contact resistance and can be neglected. (A possible exception are aluminum electrodes where our observations do not allow us to draw any conclusions about the importance of surface oxides.) We would also like to point out here that any possible change in electrode work function due to the presence of a thin surface oxide, which could affect our estimate of the value of the Schottky barrier height, is automatically taken into account in our direct measurement of the work function.

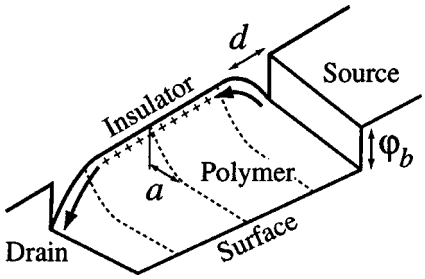

FIG. 8. Energy level diagram of holes in an ideal bottom-contact TFT. Only the valence band is sketched in the polymer. The lateral extents of the accumulation layer (a) and the depletion zone at the contacts (d) are largely exaggerated for clarity. Note that the strong band bending associated with the formation of the depletion zone (d) is only possible in the highly gate-field doped accumulation layer, and, contrary to the standard Schottky model (Ref. 33), is due to the absence rather than the presence of net space charge in this region, a peculiarity of the two-dimensional electrostatic problem with a gate electrode close by. The bands are flat in the virtually undoped bulk of the polymer. Due to electric-field-induced barrier lowering the main paths of current flow at the contacts are within a few nanometers of the insulator interface, as indicated by arrows (Ref. 21). For simplicity, barrier lowering is not shown.

Having ruled out the importance of surface oxides we now turn to two other mechanisms likely to contribute to the contact resistance: charge carrier injection as well as bulk transport in the polymer before the charge carriers reach the accumulation layer at the insulator/polymer interface. The experimental fact that for TFTs with relatively small contact effects the contact resistance is dominated by the mobility of the polymer [Fig. 7(a)] suggests that in this case bulk transport in the polymer dominates. On the other hand, the clear asymmetry between the source and drain seen in transistors with appreciable φ_b (Fig. 4) indicates that in this case injection of charge carriers at the source contact contributes predominantly to the contact resistance.[21] Therefore, our observations directly suggest a simplified low-frequency equivalent polymer TFT circuit where the conducting path between the source and drain is divided into a series of four resistive elements:

$$R_{s-d}=R_s+R_{ch}+R_d=R_i+R_b+R_{ch}+R_b. \quad (1)$$

By doing so, the source contact resistance $R_s=R_i+R_b$ is split into two parts where R_i originates from the injection of charge carriers at the reverse biased source contact and R_b from bulk transport through a narrow region in front of the contact where no accumulation layer forms due to the reasons discussed below (Fig. 8).[21,32] R_{ch} is the gate-modulated channel resistance. Furthermore, since the resistance arising from the extraction of charge carriers at the forward biased drain contact is expected to be negligible, the drain contact resistance is assumed to be entirely due to bulk transport through the narrow no-accumulation region in front of the drain, i.e., $R_d=R_b$.

In the following we discuss our results in the framework of this simple model. First, we note that whatever the exact nature of the injection mechanism is, it is reasonable to assume that the resistance due to the injection process R_i increases strongly (exponentially) with an increase in Schottky barrier height φ_b. In comparison, the φ_b dependence of the bulk resistance R_b is much weaker (see below). Therefore, one would expect there to be a critical value φ_b^* such that for barriers smaller than this critical value the bulk contribution dominates over injection ($R_b \gg R_i$), whereas for $\varphi_b > \varphi_b^*$ injection dominates the source contact resistance ($R_i \gg R_b$). From our results we infer that for polymer TFTs $\varphi_b^* \approx 0.3$ eV. For transistors with a low Schottky barrier (P3HT with Au, Ag, or Cr–Au electrodes; see Table I) we are thus in the regime where bulk transport in the polymer dominates, i.e., $R_s=R_b=R_d$, thereby explaining the symmetry observed between the source and drain [Fig. 5(a)] as well as the fact that the contact resistance is directly proportional to the inverse of the mobility [Fig. 7(a)]. However, for TFTs with a Schottky barrier exceeding φ_b^* (e.g., P3HT/Cr, F8T2/Au, F8T2/Cr–Au; see Table I) the source contact resistance is dominated by injection, i.e., $R_s \approx R_i > R_b=R_d$, and thus asymmetries are >1 in this case [Fig. 5(a)].

Next, the possible physical processes that give rise to the injection resistance R_i as well as to the bulk resistance R_b are addressed. We concentrate on the bulk contribution R_b first. Polymer material defects near the contacts that lead to narrow regions of negligible mobility or, alternatively, to regions that contain trapped positive interface charges have been invoked and could explain the occurrence of R_b in bottom-contact polymer TFTs.[21] Naturally, since in this case the resistances arise from conduction along the borders of defect-rich regions in the polymer they are inversely proportional to its mobility. (One has to keep in mind, however, that the mobility depends on the charge carrier concentration and therefore the bulk mobility is generally different from the field-effect mobility.) Such defect-rich regions at the contacts are a serious issue with respect to polycrystalline, vapor-deposited oligomers[1] because, first, the growth mode of the film can be substantially different on the insulator than on the electrode and, second, predeposited electrodes can lead to self-shadowing during the evaporation process. However, for solution-processed, less ordered polymer films these effects are generally believed to be much less pronounced. More important, in polymer TFTs the size of the defect-rich regions is not expected to depend much on the composition of the electrodes, and in particular it is not expected to depend monotonically on the Schottky barrier φ_b. Therefore, one would not expect R_b to substantially depend on the electrode material nor on φ_b, in contradiction with our results obtained for P3HT transistors with Au, Ag, Cr–Au, and Cu electrodes (Table I). We therefore seek an alternative explanation whereby R_b arises from bulk transport through a narrow depleted region in the vicinity of the contacts where no accumulation layer forms (see Fig. 8).[32] The width of this depletion layer depends on the charge carrier density N,[33] and since $N \propto |V_g|$ it implicitly depends on V_g too, which explains the V_g dependence of R_b: The larger $|V_g|$, the narrower the depletion width and therefore R_b decreases with an increase of $|V_g|$ [see P3HT/Cr–Au in Fig. 5(b)]. A conservative upper boundary of 100 nm for the depletion layer width can be estimated by inspecting potential profiles in the vicinity of the electrodes [e.g., the one for P3HT/Cr–Au in Fig. 4(a)]. Obviously, since in this picture the contact resistance is due to bulk conduction through the depleted region, R_b is proportional to μ^{-1} [Fig. 7(a)]. Important is the fact that the

depletion width also increases with an increase in Schottky barrier φ_b,[33] thus explaining the dependence of R_b on φ_b (P3HT transistors with Au, Ag, Cr–Au, and Cu electrodes in Table I).

We now focus on the interesting, injection-limited case where R_i dominates the contact resistance, which is realized in TFTs with $\varphi_b \geqslant 0.3$ eV such as P3HT with Cr electrodes and F8T2 with Au or Cr–Au electrodes. Only in this regime can the resistance originating from the injection process at the source, R_i, be measured.[21] (R_i is masked by the dominant R_b in transistors with $\varphi_b < 0.3$ eV.) Although this regime will have to be avoided for any technologically viable TFT applications, it is very interesting from a fundamental point of view since it allows one to directly study intrinsic properties of the charge carrier injection process at the source contact. A simple injection model that is often invoked as being appropriate for low-mobility organic semiconductors[9,22] is diffusion-limited thermionic emission (DLTE),[34,35] which predicts a contact resistance given by[22]

$$R_i^{\mathrm{DLTE}} \propto \mu^{-1} E^{-1} \exp[(\varphi_b - \Delta\varphi)/kT], \tag{2}$$

where E is the electric field strength at the contact and $\Delta\varphi$ is the field-induced barrier lowering. [For conjugated organic materials simple thermionic emission where $R_i^{\mathrm{TE}} \propto \exp[(\varphi_b - \Delta\varphi)/kT]$ is not applicable because in these low-mobility systems strong backflow occurs due to the large concentration of charge carriers at the interface.[34]] In connection with bottom-contact organic field-effect transistors the contact resistance has almost exclusively been modeled[20,21] and interpreted[9,10,14,16] in terms of thermionic emission models. Let us therefore try to interpret our data in the framework of such a model first. As seen from Eq. (2) the temperature dependence of diffusion-limited thermionic emission is not just governed by interface energetics, there is a contribution from the charge carrier mobility too. In the case of an activated mobility this results in an overall activation energy of the injection process of $\Delta_\mu + \varphi_b - \Delta\varphi$. However, this is in strong contrast to our experimental results. In the injection-limited regime the activation energies of R_s (and thus of R_i) of $\Delta_R = 60-140$ meV are smaller than the activation energy of the mobility as well as significantly smaller than φ_b [Fig. 7(b)]. Therefore, the observed Δ_R is definitely smaller than $\Delta_\mu + \varphi_b - \Delta\varphi \geqslant \Delta_\mu$ predicted from thermionic emission. This leads us to the important conclusion that the contact resistance in bottom-contact polymer TFTs is clearly not accounted for by a simple (diffusion-limited) thermionic emission model. We would like to point out that the applicability of thermionic emission models to disordered organic materials in general has been questioned by several authors in recent years (see, e.g., Refs. 18 and 36, and references therein).

Our results strongly suggest that alternative injection mechanisms play a dominant role in bottom-contact organic TFTs. We invoke two models here that could account for our measured low activation energies in the injection-limited regime: (thermally assisted) tunneling[37] and thermally assisted injection into a disordered organic semiconductor (insulator).[18,38,39] Essentially, in the latter model the energy distribution of initially populated sites in the organic material is displaced by σ^2/kT from the available site distribution[38] (σ is the width of the assumed Gaussian density of states), resulting in an effective, temperature-dependent activation energy of R_i of $\varphi_b - \sigma^2/kT - \Delta\varphi$ which can be considerably reduced from the barrier for injection φ_b.[18] On the other hand, since the depletion layer is expected to be very narrow, (i.e. a few nanometers, see Fig. 8) and the electric fields at the contacts are rather large, tunneling may well play a dominant part as well. (A conservative experimental lower limit for the electrical field at the source of $\approx 5\ 10^7$ V/m can be estimated from the slope of the potential profiles at the contact; see Fig. 4.)

V. CONCLUSION

In summary, the mechanisms governing the source/drain contact resistance of bottom-contact polymer TFTs have been examined experimentally by noncontact scanning-probe potentiometry. Using this microscopic technique the $I-V$ characteristics of the source/polymer as well as of the polymer/drain contacts could be measured very directly and have been found to be nonohmic for Schottky barrier heights larger than ≈ 0.3 eV. We found a clear dependence of the contact $I-V$ curves on the work function W_m of the electrodes as well as on the ionization potential I of the polymer, with a contact resistance that increases with an increase in Schottky barrier height $\varphi_b = I - W_m$. Importantly the temperature dependent measurements of the contact resistance allowed us to identify two distinct regimes. First, for electrode/polymer combinations that form bad contacts with a relatively large Schottky barrier of $\varphi_b \geqslant 0.3$ eV charge carrier injection from the source electrode into the organic semiconductor constitutes the main obstacle and dominates the contact resistance. As a main result, the surprisingly low activation energy of the order of 100 meV measured for this injection process has been found to be smaller than both the activation energy of the charge carrier mobility as well as the Schottky barrier height. This important observation rules out simple (diffusion-limited) thermionic emission models as being appropriate for a description of contact resistance in bottom-contact polymer TFTs. Second, for good contacts with relatively small overall contact resistance ($\leqslant 50$ kΩ cm) the source and drain contact resistances were found to be equal and they showed exactly the same temperature dependence as the charge carrier mobility of the polymer. Therefore, a bulk transport process in the polymer, most likely transport through a narrow depleted region in front of the electrodes, dominates the source as well as the drain contact resistance in TFTs with Schottky barrier $\varphi_b < 0.3$ eV. Our results underscore the importance of the charge carrier mobility for the injection process in organic TFTs. The obvious routes to reduce contact resistance effects by matching the work function of the electrodes with the ionization potential of the polymer as closely as possible have thus to be complemented by efforts to enhance the bulk charge carrier mobility in the vicinity of the contacts as well as by efforts to reduce the lateral extent of the depleted layer. Apart from more conventional approaches such as tuning the electrode work function, e.g., by means of self-assembled charge transfer materials,[40] methods such as selective doping, predeposition

of a highly ordered ultrathin layer,[41] or molecular-scale engineering of interlayers to form stepped and graded electronic profiles at the contacts[42] will have to be explored more intensively.

Finally, a clear picture of the contact resistance in ''conventional'' organic transistors is a first step towards viable organic TFTs of submicrometer (possibly molecular) dimensions.

ACKNOWLEDGMENTS

One of the authors (L.B.) thanks the Swiss National Science Foundation for funding under an Advanced Researcher fellowship. This work was financially supported by the Engineering and Physical Sciences Research Council and the Epson Cambridge Laboratory. The authors would like to thank P. P. Ruden (University of Minnesota, Minneapolis) for discussions. R. S. Loewe and R. D. McCullough (Carnegie Mellon University, Pittsburgh) as well as Merck Chemicals Ltd. provided the P3HT, and the F8T2 was supplied by the Dow Chemical Company.

[1] C. D. Dimitrakopoulos and P. R. L. Malenfant, Adv. Mater. (Weinheim, Ger.) **14**, 99 (2002).
[2] J. Zaumseil, T. Someya, Z. Bao, Y.-L. Loo, R. Cirelli, and J. A. Rogers, Appl. Phys. Lett. **82**, 793 (2003).
[3] N. Stutzmann, R. H. Friend, and H. Sirringhaus, Science **299**, 1881 (2003).
[4] In the wide-channel limit transistor currents scale with the transistor width, i.e., the actual contact resistance r_c is inversely proportional to the channel width W, $r_c \propto W^{-1}$. Therefore, it is convenient to use the channel-length independent product of contact resistance and channel width, $R_c = r_c W$, as a measure of the contact resistance.
[5] L. Torsi, A. Dodabalapur, and H. E. Katz, J. Appl. Phys. **78**, 1088 (1995).
[6] G. Horowitz, R. Hajlaoui, D. Fichou, and A. El Kassmi, J. Appl. Phys. **85**, 3202 (1999).
[7] H. Sirringhaus, N. Tessler, D. S. Thomas, P. J. Brown, and R. H. Friend, Adv. Solid State Phys. **39**, 101 (1999).
[8] T. W. Kelley and C. D. Frisbie, J. Vac. Sci. Technol. B **18**, 632 (2000).
[9] A. B. Chwang and C. D. Frisbie, J. Phys. Chem. B **104**, 12202 (2000).
[10] P. V. Necliudov, M. S. Shur, D. J. Gundlach, and T. N. Jackson, J. Appl. Phys. **88**, 6594 (2000).
[11] H. Sirringhaus, T. Kawase, R. H. Friend, T. Shimoda, M. Inbasekaran, W. Wu, and E. P. Woo, Science **290**, 2123 (2000).
[12] K. Seshadri and C. D. Frisbie, Appl. Phys. Lett. **78**, 993 (2001).
[13] L. Bürgi, H. Sirringhaus, and R. H. Friend, Appl. Phys. Lett. **80**, 2913 (2002).
[14] R. A. Street and A. Salleo, Appl. Phys. Lett. **81**, 2887 (2002).
[15] H. Klauk, G. Schmid, W. Radlik, W. Weber, L. Zhou, C. D. Sheraw, J. A. Nichols, and T. N. Jackson, Solid-State Electron. **47**, 297 (2003).
[16] P. V. Necliudov, M. S. Shur, D. J. Gundlach, and T. N. Jackson, Solid-State Electron. **47**, 259 (2003).
[17] J. Zaumseil, K. W. Baldwin, and J. A. Rogers, J. Appl. Phys. **93**, 6117 (2003).
[18] T. van Woudenbergh, P. W. M. Blom, M. C. J. M. Vissenberg, and J. N. Huiberts, Appl. Phys. Lett. **79**, 1697 (2001).
[19] N. Tessler and Y. Roichman, Appl. Phys. Lett. **79**, 2987 (2001).
[20] A. Bolognesi, A. Di Carlo, and P. Lugli, Appl. Phys. Lett. **81**, 4646 (2002).
[21] T. Li, P. P. Ruden, I. H. Campbell, and D. L. Smith, J. Appl. Phys. **93**, 4017 (2003).
[22] Y. Shen, M. W. Klein, D. B. Jacobs, J. C. Scott, and G. G. Malliaras, Phys. Rev. Lett. **86**, 3867 (2001).
[23] H. Sirringhaus, N. Tessler, and R. H. Friend, Science **280**, 1741 (1998).
[24] R. S. Loewe, S. M. Khersonsky, and R. D. McCullough, Adv. Mater. (Weinheim, Ger.) **11**, 250 (1999).
[25] A. Salleo, M. L. Chabinyc, M. S. Yang, and R. A. Street, Appl. Phys. Lett. **81**, 4383 (2002).
[26] We used either Pt/Ir coated Si probes from Digital Instruments (model SCM-PIT, $f_r \approx 75$ kHz) or Au coated probes from MikroMasch (model NSC14/Cr–Au, $f_r \approx 160$ kHz).
[27] By doing so we neglect any interfacial dipole layer that may form when the organic material is deposited on the electrode which alters the barrier to $\varphi_b = I - W_m - \delta$. However, almost all organic-material-on-metal contacts exhibit negative values for δ (which therefore increases the hole-injection barrier) and there normally is a monotonous decrease of δ with an increase of W_m with a slope clearly smaller than 1 (after Ref. 28). Therefore, it is very reasonable to assume that trends in $I - W_m$ correctly reproduce trends in $I - W_m - \delta$.
[28] H. Ishii, K. Sugiyama, E. Ito, and K. Seki, Adv. Mater. (Weinheim, Ger.) **11**, 605 (1999).
[29] J. Kanicki, F. R. Libsch, J. Griffith, and R. Polastre, J. Appl. Phys. **69**, 2339 (1991).
[30] S. Luan and G. W. Neudeck, J. Appl. Phys. **72**, 766 (1992).
[31] S. F. Nelson, Y.-Y. Lin, D. J. Gundlach, and T. N. Jackson, Appl. Phys. Lett. **72**, 1854 (1998).
[32] T. Li, J. W. Balk, P. P. Ruden, I. H. Campbell, and D. L. Smith, J. Appl. Phys. **91**, 4312 (2002).
[33] S. M. Sze, *Physics of Semiconductor Devices* (Wiley, New York, 1981).
[34] J. G. Simmons, Phys. Rev. Lett. **15**, 967 (1965).
[35] P. R. Emtage and J. J. O'Dwyer, Phys. Rev. Lett. **16**, 356 (1966).
[36] Y. Preezant and N. Tessler, J. Appl. Phys. **93**, 2059 (2003).
[37] E. L. Wolf, *Principles of Electron Tunneling Spectroscopy* (Oxford University Press, New York, 1985).
[38] Y. N. Gartstein and E. M. Conwell, Chem. Phys. Lett. **255**, 93 (1996).
[39] V. I. Arkhipov, E. V. Emelianova, Y. H. Tak, and H. Bässler, J. Appl. Phys. **84**, 848 (1998).
[40] D. J. Gundlach, L. Jia, and T. N. Jackson, IEEE Electron Device Lett. **22**, 571 (2001).
[41] T. Hassenkam, D. R. Greve, and T. Bjørnholm, Adv. Mater. (Weinheim, Ger.) **13**, 631 (2001).
[42] P. K. H. Ho, J.-S. Kim, J. H. Burroughes, H. Becker, S. F. Y. Li, T. M. Brown, F. Cacialli, and R. H. Friend, Nature (London) **404**, 481 (2000).